

# The MX2 macromolecular crystallography beamline: a wiggler X-ray source at the LNLS

Beatriz G. Guimarães,<sup>a\*</sup> Lucas Sanfelici,<sup>a</sup> Regis T. Neuenschwander,<sup>a</sup> Flávio Rodrigues,<sup>a</sup> Walan C. Grizolli,<sup>a</sup> Marco A. Raulik,<sup>a</sup> James R. Piton,<sup>a</sup> Bernd C. Meyer,<sup>a</sup> Alessandro S. Nascimento<sup>b</sup> and Igor Polikarpov<sup>b\*</sup>

<sup>a</sup>Laboratório Nacional de Luz Síncrotron (LNLS), Campinas, SP, Brazil, and <sup>b</sup>Instituto de Física de São Carlos, Universidade de São Paulo, Av. Trabalhador São-carlense, 400 São Carlos, SP 13560-970, Brazil. E-mail: beatriz@lnls.br, ipolikarpov@ifsc.usp.br

The Brazilian Synchrotron Light Laboratory [Laboratório Nacional de Luz Síncrotron (LNLS), Campinas, SP, Brazil] is the first commissioned synchrotron light source in the southern hemisphere. The first wiggler macromolecular crystallography beamline (MX2) at the LNLS has been recently constructed and brought into operation. Here the technical design, experimental set-up, parameters of the beamline and the first experimental results obtained at MX2 are described. The beamline operates on a 2.0 T hybrid 30-pole wiggler, and its optical layout includes collimating mirror, Si(111) double-crystal monochromator and toroidal bendable mirror. The measured flux density at the sample position at 8.7 eV reaches  $4.8 \times 10^{11}$  photons  $s^{-1}$   $mm^{-2}$  (100 mA) $^{-1}$ . The beamline is equipped with a MarResearch Desktop Beamline Goniostat (MarDTB) and  $3 \times 3$  MarMosaic225 CCD detector, and is controlled by a customized version of the *Blu-Ice* software. A description of the first X-ray diffraction data sets collected at the MX2 LNLS beamline and used for macromolecular crystal structure solution is also provided.

**Keywords:** macromolecular crystallography; wiggler beamline; protein X-ray diffraction.

## 1. Introduction

The new era of structural molecular biology claims for structural comprehension of molecular phenomena in their cellular contexts, usually requiring the study of macromolecular assemblies, such as protein homo/hetero complexes or protein–nucleic acid complexes. Since X-ray crystallography remains as the method of choice for gathering this structural information, accounting for more than 83% of the macromolecular structures currently deposited in the Protein Data Bank (PDB), pressure lies on having better X-ray data from increasingly poorly diffracting crystals. The inherent experimental difficulties of the macromolecular X-ray diffraction experiments have been overcome in part by the use of increasingly brighter synchrotron sources. The improvements in synchrotron stations dedicated to macromolecular crystallography (MX) data collection include the use of insertion devices (IDs), leading to higher flux density even in the limiting wavelengths.

A number of ID-equipped synchrotron stations are currently available and their outstanding relevance to structural biology can be evaluated in the BIOSYNC database (<http://biosync.rcsb.org/BiosyncStat.html>; Jiang & Sweet, 2004). In 2003, 75% of the macromolecular structures solved and deposited in the PDB took advantage of synchrotron

sources. In 2007, according to the BIOSYNC database, 6807 structures were solved and deposited in the PDB, with 5504 of these deposited structures using synchrotron sources, corresponding to 81% of the total. Furthermore, comparing the statistics from the National Synchrotron Light Source (NSLS) as an example, the recently set up and ID-equipped X29 beamline (Shi *et al.*, 2006) alone was used in 32% of the total deposited structures solved at the light source and this tendency seems to be followed by the other synchrotron sources.

The Brazilian Synchrotron Light Laboratory [Laboratório Nacional de Luz Síncrotron (LNLS), Campinas, SP, Brazil] is the first commissioned synchrotron light source in the southern hemisphere and has been extensively used by the international scientific community, especially by research groups from Latin America, since 1997 (Rodrigues *et al.*, 1998). The LNLS is a 1.37 GeV source operating at a maximum current of 250 mA with a critical photon energy reaching 2.08 keV. The current LNLS beamline dedicated to macromolecular crystallography (D03B-MX1) (Polikarpov *et al.*, 1998) was commissioned in 1997 and has been widely used since then. According to BIOSYNC statistics, based on deposited file headers, to date 123 structures have been solved using this beamline. Although demand for macromolecular diffraction data collection is increasing rapidly in Brazil and

Latin America, the LNLS storage-ring characteristics limit the number of conducted structural studies, partly as a result of the fact that the beam flux at wavelengths shorter than  $1.0 \text{ \AA}$  is low and the design of the MX1 beamline is inadequate for typical MAD experiments. In addition, the flux density of  $4.5 \times 10^{10} \text{ photons s}^{-1} \text{ mm}^{-2}$  ( $100 \text{ mA}$ ) $^{-1}$  at  $8.7 \text{ eV}$  sets limits on the crystal size to be used for X-ray diffraction data collection even for well diffracting crystals.

In this work we describe the set-up, experimental parameters and first results obtained at the W01B-MX2, an ID-equipped beamline dedicated to macromolecular crystallography. The measured flux density reaches  $4.8 \times 10^{11} \text{ photons s}^{-1} \text{ mm}^{-2}$  ( $100 \text{ mA}$ ) $^{-1}$  at  $8.7 \text{ eV}$ . Some successful MAD/SAD experiments as well as native diffraction data set collection are described.

## 2. Hardware set-up

### 2.1. Beamline set-up

W01B-MX2 is the first LNLS beamline based on an insertion device. Owing to the storage-ring characteristics, a wiggler was the choice to improve the photon flux density of the beamline, since undulators, at the low- and medium-energy synchrotron rings, would not be capable of producing synchrotron radiation in the X-ray region needed for macromolecular diffraction data collection. The 2.0 T hybrid multipolar wiggler was purchased from STI Optronics (Seattle, USA). A minimum gap of 22 mm generates the peak magnetic field and a total of 30 poles accounts for the length of the magnetic assembly (2.70 m). Various changes to the light-source subsystems were implemented prior to the wiggler installation, including an upgrade of the storage-ring RF system. The wiggler vacuum chamber was designed and built at the LNLS and consists of a 3 m-long stainless steel tube shaped into an approximately elliptical form, with pumping ports at its ends. The chamber inner surface is NEG-coated in order to improve the pressure in the long thin chamber. At the beamline front-end a graphite filter absorbs most of the thermal power generated by the wiggler. It consists of a  $250 \text{ \mu m}$  HOPG foil clamped between two water-cooled copper plates, assuring the dissipation, approximately, of a power of 1300 W.

The MX2 optical layout consists of a collimating mirror that sends parallel synchrotron beam onto the two flat Si(111) monochromator crystals (Fig. 1). The monochromatic radiation after the monochromator is refocused by a toroidal bendable mirror. Similar optical and experimental design have been used on several other synchrotron facilities around the world, including the GPCCC beamline at CAMD (USA;

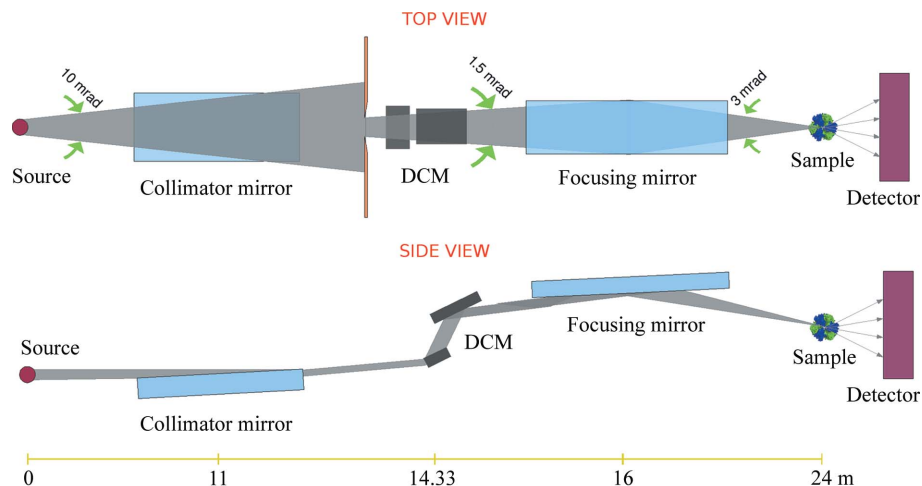


**Figure 1**  
Optical scheme of the LNLS MX2 wiggler beamline. Top and side views are provided.

Miller *et al.*, 2001), B114 at BESSY (Germany; [http://www.mx.bessy.de/userguide/beamlines/bl1/141\\_software.shtml](http://www.mx.bessy.de/userguide/beamlines/bl1/141_software.shtml)), BW6 at DESY (Germany; Buth *et al.*, 1996) and beamline 10 at SRS (UK; Cianci *et al.*, 2005), to name a few. Mirrors were purchased from SESO (France) and the silicon monochromator crystals were cut at the LNLS with dimensions of  $8 \times 45 \times 45 \text{ mm}$  (for the first crystal) and  $8 \times 35 \times 110 \text{ mm}$  (for the second crystal). The accuracy of the (111) plane orientation is  $\pm 0.1^\circ$ . The beamline optical design was optimized to a maximum divergence of 3 mrad on the sample position with a 2:1 focusing ratio (Fig. 1). The first-mirror (990 mm of rhodium-coated ULE glass) specifications were defined in order to guarantee 90% reflectivity of 15 keV photons for an incident angle of 4.0 mrad. The monochromator crystals are mounted onto a Huber goniometer and vertical translation of the second crystal provides a fixed exit beam. Both the collimating mirror and the monochromator first crystal are water cooled. Cooling systems were designed taking into account the calculated absorbed power, of approximately 25 W and 35 W for the first mirror and monochromator crystal, respectively. The focusing toroidal mirror consists of 1200 mm-long rhodium-coated silicon. A mechanical bender tunes its longitudinal radius. Mirrors and monochromator mechanics are mounted on isolated concrete blocks to assure optical stability.

The LNLS MX2 beamline components are schematically represented in Fig. 2. Fluorescent screens are placed along the beamline for visual inspection of the beam (3, 7, 12 in Fig. 2), and the outcome photocurrent of a  $5 \text{ \mu m}$ -thick Al foil placed downstream of the monochromator (9 in Fig. 2) is used to tune the second crystal pitch. A vertically motorized tungsten-wire monitor allows analysis of the beam centroid and profile upstream of the collimating mirror (3 in Fig. 2) and a copper-blades beam-position monitor (BMP) is placed downstream of the mirror (5 in Fig. 2). Finally, to track vertical and horizontal displacement of the beam, a quadrant photodiode-based BMP was placed a few centimeters upstream of the sample position (14 in Fig. 2). The quadrant BMP was designed and built based

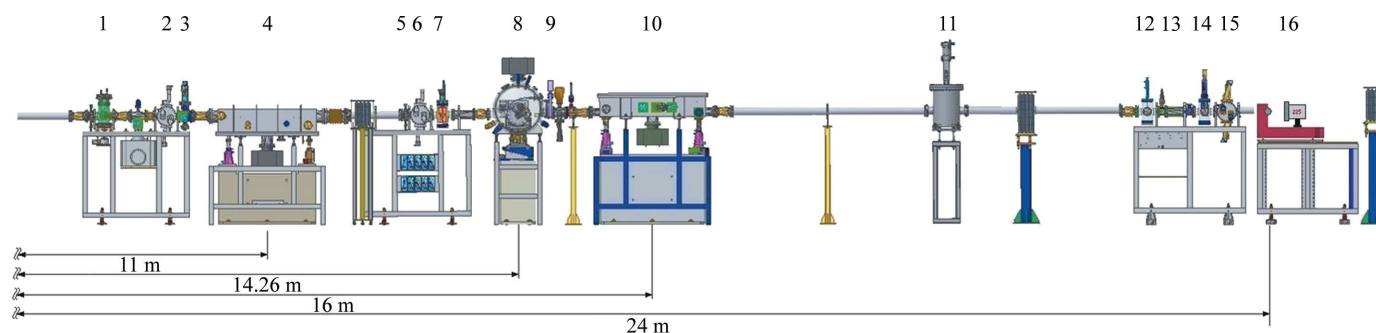


**Figure 2**

Schematic view of the LNLS MX2 beamline. Numbers at the top indicate the components as follows: (1) graphite filter; (2, 6, 15) sets of slits; (3) vertical beam-profile monitor and alumina screen; (4) collimating mirror; (5) vertical beam-position monitor; (7) aluminium screen; (8) double-crystal monochromator; (9) beam-intensity monitor; (10) focusing mirror; (11) monochromatic photon shutter; (12) fluorescent screen; (13) attenuators set; (14) quadrant beam-position monitor; (16) goniostat and MarCCD detector. The distances from the optical elements and sample position to the source are indicated at the bottom of the figure.

on the model developed by Alkire and co-workers (Alkire *et al.*, 2000).

Six 125  $\mu\text{m}$ -thick beryllium windows separate the vacuum sections, four of them placed at the extremities of the mirror chambers. Pressure along the beamline is kept at approximately  $5 \times 10^{-9}$  mbar at the front-end and first mirror,  $7 \times 10^{-9}$  mbar at the monochromator and  $5 \times 10^{-9}$  mbar at the second mirror. Downstream of the second mirror chamber a mechanical pump keeps the pressure at approximately  $10^{-3}$  mbar along the beam path until the experimental station.

## 2.2. Experimental station

The MX2 beamline is equipped with a MarResearch Desktop Beamline Goniostat (MarDTB) providing a high-precision  $\varphi$ -axis movement and automatic positional and directional alignment and adaptive beam optimization. The desktop motorized slits permit an automated beam shape optimization with individual settings for horizontal and vertical beam width, varying from 0 to 5 mm with 2.5  $\mu\text{m}$  resolution. The manual crystal mounting is accompanied by a CCD microscope placed along the beam path, with an offset of  $20^\circ$  and coupled to a 4" LCD monitor;  $\Phi$ -axis with motor-driven crystal centering allows mouse-click sample centering.

A  $3 \times 3$  MarMosaic225 CCD detector is mounted on the desktop, providing a 50625  $\text{mm}^2$  X-ray-sensitive surface. The read noise of  $6 e^-$  for 2 s readout allows reliable data collection in a very short time, consistent with the beamline high-photon-flux density. A Cryojet from Oxford Instruments and an Amptek XR100CR fluorescence detector complete the experimental station. The user-accessible experimental hutch is equipped with a key-based security system, which guarantees safety, even to the less experienced user.

## 3. Control software

At present, most of the LNLS MX2 beamline components are controlled by a customized version of the *Blu-Ice* software (McPhillips *et al.*, 2002), developed by the Macromolecular Crystallography Group at the Stanford Synchrotron Radiation

Laboratory (<http://smb.slac.stanford.edu/public/research/developments/blu-ice/>). The exceptions are the MarDTB goniostat and the MarCCD detector. Thus, the beamline alignment, energy selection and fluorescence scans are controlled *via* the *Blu-Ice* GUI, whereas crystal centering and X-ray data collection are carried out *via* the MarResearch software. The *Blu-Ice* software makes use of a well designed structure for controlling hardware in a heterogeneous computing environment system. The user interface of *Blu-Ice* has been developed in Tcl/Tk (Tool Command Language), a multiplatform scripting language. It makes use of a package termed DCS, Distributed Control System, composed of hardware servers (DHS) and a unique DCS server (DCSS). The DHS is responsible for the execution of low-level code. Since DCS uses the TCP/IP protocol, it is independent from the operational system of the machine. The DCSS controls all the messages between the *Blu-Ice* graphical interface and that of the DHS. It routes an incoming message from the users interface to the proper DHS based on the device it refers to. It also prevents the hardware from being damaged by controlling all the flow of commands. Fig. 3 shows an example of the *Blu-Ice* GUI frames. The *Blu-Ice* GUI allows the user to easily perform fluorescence scans and to select the data collection energy. Tuning of the pitch of the monochromator second crystal can also be easily performed when needed. For example, energy change from 7 to 12 keV and pitch optimization can be carried out in a few minutes. Integration of diffraction data collection control into the *Blu-Ice* software is in progress. DHSs have been written and are currently being tested. Users X-ray data are stored in the hard disks of the beamline linux machines for two weeks. Backups are mainly carried out using external hard disks, but data can also be retrieved by the users *via* ftp.

## 4. Experimental parameters

The MX2 beamline operates in the energy range 5 to 15 keV with maximum flux at 8 keV. Fig. 4(a) shows the flux density as a function of energy measured at the sample position. Low-energy X-ray photons are absorbed by the beryllium windows,

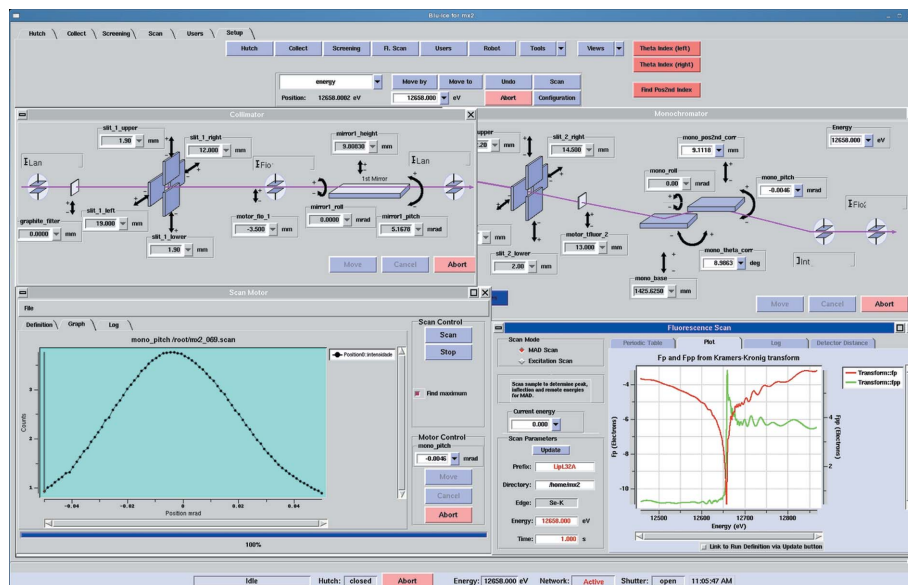


**Figure 3** *Blu-Ice* graphical user interface. At the top the frames show the interface for controlling the mirror angles and position and the monochromator. At the bottom the rocking curve of the monochromator second crystal (left-hand side) and the results of a fluorescence scan (right-hand side) are shown.

and the collimating mirror energy cut-off limits the photon flux at high energy. Beamline energy resolution capacity was determined by measuring the  $\text{KMnO}_4$  ‘white line’ at low energies (Fig. 4b). An average value of  $\Delta E/E = 2.2 \times 10^{-4}$  was obtained based on the measured full width at half-maximum (FWHM) and the natural width of the Mn core level. Changing the vertical aperture of pre-monochromator slits produces no significant effect on the beamline resolution, indicating good collimation of the first-mirror outgoing beam. The toroidal mirror focuses the beam to a spot size (FWHM) at the sample position of  $0.17 \times 0.53$  mm (vertical  $\times$  horizontal) at a synchrotron radiation energy of 8 keV. The experimentally determined size of the focused beam agrees favorably with the theoretical value of  $0.097 \times 0.461$  mm for the beam size at the same energy of X-ray radiation, obtained by simulation using the ray-tracing program *XOP/Shadow* (Welnak *et al.*, 1992). The focused beam profile at the synchrotron radiation energy of 8 keV is shown in Fig. 5.

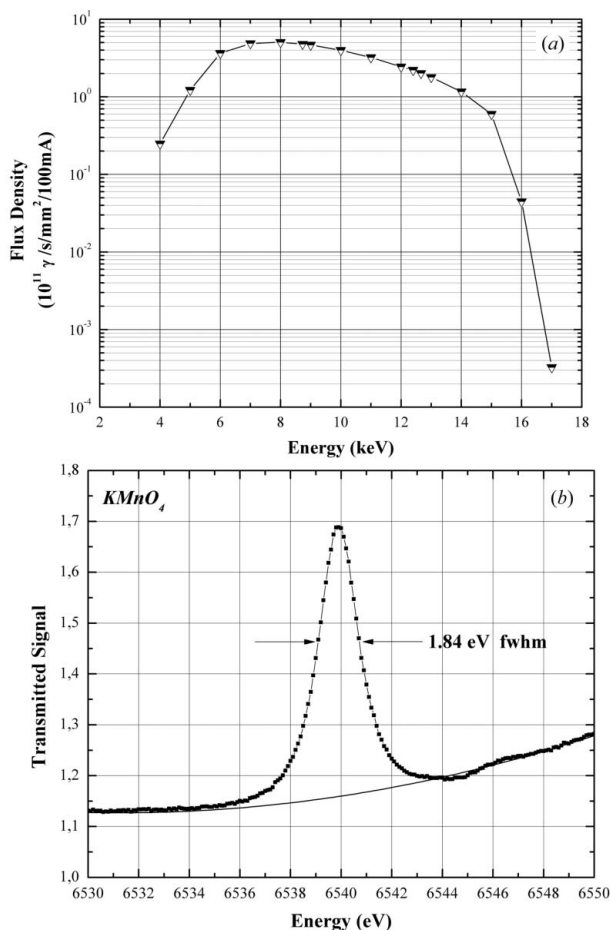


**Figure 4** Photon flux and resolution of the MX2 beamline. (a) Experimentally determined flux density as a function of energy at the sample position. (b)  $\text{KMnO}_4$  ‘white line’ at 6539 eV.

simulation using the ray-tracing program *XOP/Shadow* (Welnak *et al.*, 1992). The focused beam profile at the synchrotron radiation energy of 8 keV is shown in Fig. 5.

### 5. First X-ray crystallographic results

A number of native structures have been solved on the MX2 beamline, including a complex between human interleukin 22 and its receptor R1, solved at 1.9 Å resolution (PDB entry 3DLQ; Bleicher *et al.*, 2008) and a double mutant of the

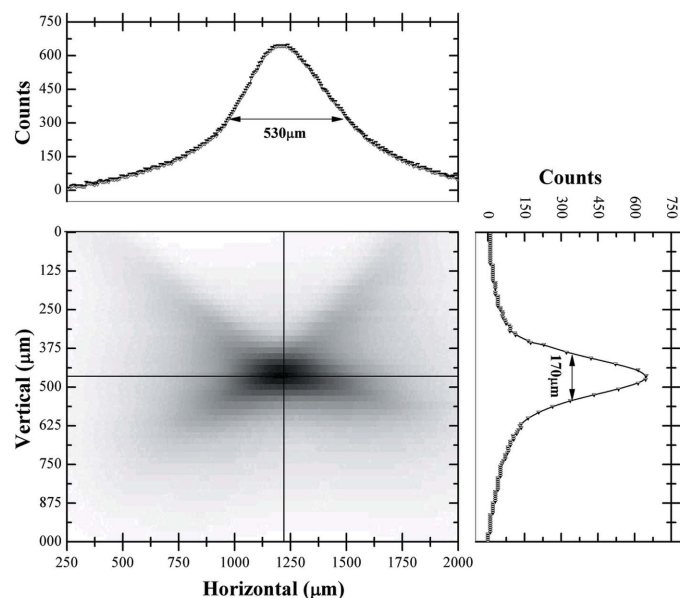


**Figure 5** Beam profile at the sample position. The experimentally determined spot size (FWHM) at 8 keV is  $0.17 \times 0.53$  mm (vertical  $\times$  horizontal).

**Table 1**

First X-ray data sets collected at the LNLS MX2 beamline.

Values in parentheses refer to the highest resolution shell.

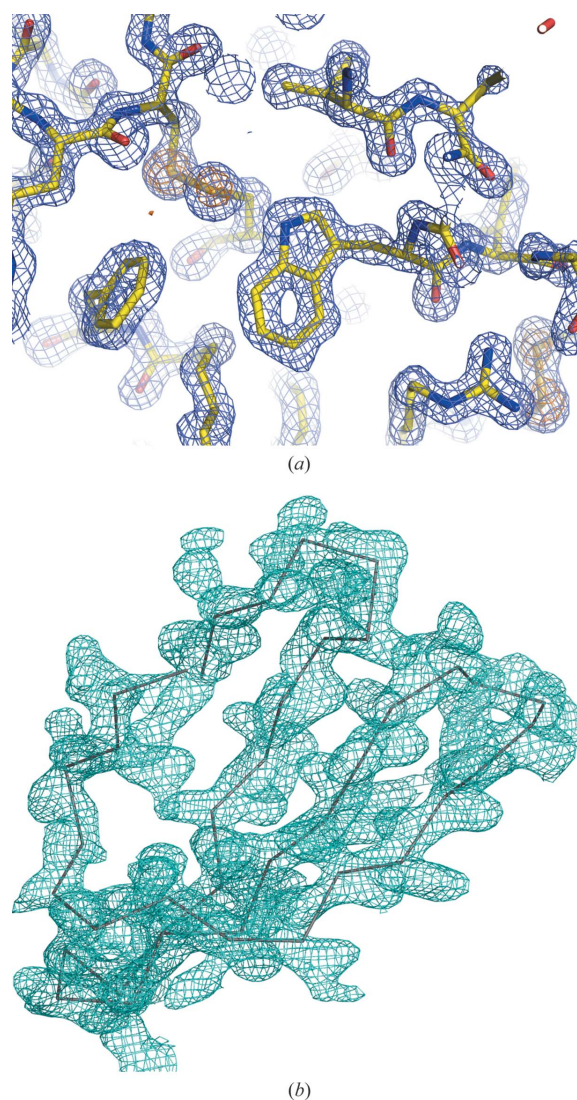
	HEWL – native	HEWL – Cs	SAD – SeMet
Wavelength (Å)	1.46	1.46	0.9795
Space group	$P4_32_12$	$P4_32_12$	$P2_12_12_1$
Unit-cell parameters (Å)	$a = b = 78.68, c = 36.92$	$a = b = 78.31, c = 37.08$	$a = 78.95, b = 86.87, c = 132.42$
$\Delta\varphi$ rotation (°)	1.00	1.00	0.7
Resolution range (Å)	55.64–1.35 (1.42–1.35)	55.38–1.60 (1.69–1.60)	53.45–1.99 (2.10–1.99)
Data collection time (s)	2.0	2.0	60.0
Total reflections	630496 (36088)	347542 (13295)	714735 (88974)
Unique reflections	25761 (3431)	15033 (1637)	60735 (8497)
Redundancy	24.5	23.1 (8.1)	6.1 (5.4)
$R_{\text{merge}}$ (%)	7.8 (71.9)	9.5 (61.5)	11.6 (37.9)
$R_{\text{pim}}$ (%)	2.1 (32.9)	2.6 (32.9)	3.6 (12.7)
Completeness (%)	98.8 (92.3)	95.4 (73.7)	95.9 (94.0)
$I/\sigma(I)$	31.1 (2.7)	26.6 (2.4)	19.3 (5.3)

human transthyretin solved at 1.38 Å resolution (PDB entry 3DGD). In the following sections we describe some examples of protein structures solved using SAD and MAD techniques.

### 5.1. SAD phasing

**5.1.1. Sulfur SAD phasing.** A number of successful cases of macromolecular phasing utilizing the weak anomalous signal of intrinsic S atoms present in cysteine and methionine residues have been reported (for example, Pal *et al.*, 2008; Wang *et al.*, 2006). This approach requires both a well diffracting crystal and a stable source. To conduct the experiment, we used a single native HEWL crystal for data collection conducted at the MX2 wiggler beamline. A complete and redundant data set was collected (see Table 1) and then integrated and scaled using *MOSFLM* (Leslie, 1992) and *SCALA* (Collaborative Computational Project, Number 4, 1994). *SHELXD* (Schneider & Sheldrick, 2002) was used to find the weak anomalous scatterers truncating the resolution at 1.9 Å. The best solution found after 1000 trials resulted in a  $CC/CC_{\text{weak}}$  of 32.99/16.84 and clear enantiomorph discrimination after phasing in *SHELXE*. After 50 cycles of model building in *ARP/wARP* (Lamzin *et al.*, 2001), 127 out of the 129 residues were built without human interference. The entire process of data reduction, phasing and model building took no more than 4 h. The built model (deposited in the PDB with entry 3EXD), and representative example of both anomalous and  $2F_{\text{obs}} - F_{\text{calc}}$  electron density maps are shown in Fig. 6(a).

**5.1.2. Quick cryo-soaking approach.** A number of derivatization techniques have been recently developed to solve the structures, which cannot be solved by molecular replacement methods. These techniques are particularly useful when MAD experiments cannot be conducted or for crystals that do not diffract at high resolution (Dauter *et al.*, 2000; Nagem *et al.*, 2001; Banumathi *et al.*, 2003; Girard *et al.*, 2003; Xie *et al.*, 2004). One very successful technique implemented at the LNLS is quick cryo-soaking, which takes advantage of the introduction of a high concentration of anomalous scatterers directly into the cryo-protecting solution prior to flash-cooling of protein crystals for X-ray data collection (Dauter *et al.*,

**Figure 6**

(a) Crystal structure of HEWL automatically built by *ARP/wARP* after phasing using the sulfur signal. The anomalous map is shown in orange countered at  $4\sigma$  whereas the  $2F_{\text{obs}} - F_{\text{calc}}$  electron density map is shown in blue contoured at  $1.5\sigma$ . (b) Electron density map ( $2F_{\text{obs}} - F_{\text{calc}}$ ) calculated from SAD experimental phases of a *Leptospira interrogans* putative lipoprotein crystal contoured at  $1.2\sigma$  (cyan). The quality of the map allowed automatic building of most of the polypeptide chain (gray). The figure was prepared using *PYMOLE* (DeLano, 2002).

2000; Nagem *et al.*, 2001, 2003, 2005). This allows heavy atom (*e.g.* I, Cs, Gd) diffusion into the crystal lattice and their rapid binding to the surface of macromolecules within it, enabling sufficient phasing power to solve novel structures from typical protein crystals (Nagem *et al.*, 2002, 2004; Golubev *et al.*, 2004; Rojas *et al.*, 2004; Krauchenco *et al.*, 2004).

During commissioning of the MX2 beamline, we performed phasing of test protein crystals using the quick cryo-soaking approach. A single HEWL tetragonal crystal of typical size 100  $\mu\text{m}$  was soaked in a mother liquor solution containing 0.5 M CsCl<sub>2</sub> and 15% ethylene glycol for for 1 min. Experimental parameters of the data set collected from the flash-frozen crystal are shown in Table 1.

Two Cs sites were found using *SHELXD* after 1000 trials, truncating the resolution at 2.2 Å. The best solution yielded a CC/CC<sub>weak</sub> of 31.88/17.14 and a clear discrimination between the enantiomorphs was achieved as well using *SHELXE*. The improvements in the anomalous signal by the addition of the anomalous scatterers during the cryo-soaking are readily observed (see supplementary Fig. S1<sup>1</sup>) with the increase in the average anomalous signal, taken as  $\langle |F^+| - |F^-| \rangle / \langle F \rangle$ , from 0.08 for the native data set to 0.14 in the quick cryo-soaking data set.

## 5.2. SAD and MAD phasing from selenomethionine-labeled crystals

Selenomethionine-labeled crystals of a putative lipoprotein from *Leptospira interrogans* were grown in 0.2 M LiSO<sub>4</sub>, 0.1 M Tris-HCl pH 8.5 and 15% PEG 4000. Anomalous scattering factors were derived from the emission fluorescence spectrum of the crystal using the program *CHOOCH* (Evans & Pettifer, 2001). Then, diffraction data were collected at a single wavelength (0.9795 Å) corresponding to the maximum of  $f''$ . Table 1 summarizes the data collection statistics. All 14 expected selenium atoms were located by the hybrid substructure search method (Grosse-Kunstleve & Adams, 2003) and initial phasing was calculated using *Phaser* (McCoy *et al.*, 2007). Density modification was carried out using *RESOLVE* (Terwilliger, 2003) which was also used to build and refine a preliminary model. Further automatic model building was carried out using *ARP/wARP* (Lamzin *et al.*, 2001). Fig. 6(b) shows the electron density map obtained from experimental phases. The asymmetric unit is composed of two monomers and the final refined model comprises 814 residues. Refinement statistics and analysis of the structure were recently published (Giuseppe *et al.*, 2008) and atomic coordinates were deposited in the PDB (ID 3BWS).

Multiwavelength anomalous diffraction data were collected from selenomethionine-labeled crystals of a soluble *Xanthomonas axonopodis* protein (Guzzo & Farah, 2009). A MAD data set was collected at three different wavelengths for a single crystal that diffracted to 1.85 Å. These data sets were initially indexed in space group *P6<sub>1</sub>22*, though symmetry was

reduced to *P6<sub>1</sub>* at a later stage during model refinement. All expected selenium sites were found for the single monomer in the *P6<sub>1</sub>22* asymmetric unit using *SHELXD* (Schneider & Sheldrick, 2002). Se sites were refined using *SHARP* (La Fortelle & Bricogne, 1997) which produced the first phase estimates up to 1.9 Å. Phases were refined by density modification using the programs *SOLOMON* (Abrahams & Leslie, 1996) and *DM* (Cowtan, 1994). Automatic model building was carried out with *ARP/wARP* (Lamzin *et al.*, 2001). Structural refinement of the atomic model of the two monomers in the *P6<sub>1</sub>* asymmetric unit was performed using *REFMAC* (Murshudov *et al.*, 1997), *CNS* (Brünger *et al.*, 1998) and *COOT* (Emsley & Cowtan, 2004).

## 6. Conclusions and perspectives

MX2 is the first dedicated protein crystallography wiggler beamline in Latin America suitable both for native and anomalous data collection. Its technical parameters and characteristics as well as the first X-ray diffraction data sets collected at the beamline assure that it can be very useful for macromolecular structure determination. The beamline will provide an important technical support for rapidly growing research in structural molecular biology in Brazil and other Latin American countries. In the future both hardware and software capabilities of the beamline will be extended by installing a higher-flux fluorescence detector with better energy resolution and allowing for better integration of the software for beamline operation, data collection and data processing. Furthermore, the feasibility of sample-changer installation and remote data collection are currently being studied. Experience with the beamline operation and data collection at the first dedicated wiggler protein crystallography beamline will be useful for the development and installation of the ID macromolecular crystallography beamlines to follow. One also could expect that MX2 capabilities for MAD data collection will increase the number of novel structures solved in this part of the world.

We are very grateful to the Advanced Light Source team for helpful discussions during the assembly and commissioning of the beamline, in particular to James Holton, Alastair MacDowell, Corie Ralston and Thomas Earnest. We are very grateful to Scott McPhilips and the *Blu-Ice* developers' team for providing the software code and for their huge help with *Blu-Ice* installation and customization. We are thankful to Robert Sweet for a number of useful suggestions and friendly support. We are also indebted to Shaker Chuck Farah, Lucas Bleicher and Marcelo V. Liberato for their kindness in providing X-ray diffraction data sets collected at the LNLS MX2 beamline.

## References

- Abrahams, J. P. & Leslie, A. G. W. (1996). *Acta Cryst.* **D52**, 30–42.
- Alkire, R. W., Rosenbaum, G. & Evans, G. (2000). *J. Synchrotron Rad.* **7**, 61–68.
- Banumathi, S., Dauter, M. & Dauter, Z. (2003). *Acta Cryst.* **D59**, 492–498.

<sup>1</sup> Supplementary data for this paper are available from the IUCr electronic archives (Reference: H15587). Services for accessing these data are described at the back of the journal.

- Bleicher, L., Moura, P. R., Watanabe, L., Colau, D., Dumoutier, L., Reanault, J.-C. & Polikarpov, I. (2008). *FEBS Lett.* **582**, 2985–2992.
- Brünger, A. T., Adams, P. D., Clore, G. M., DeLano, W. L., Gros, P., Grosse-Kunstleve, R. W., Jiang, J.-S., Kuszewski, J., Nilges, M., Pannu, N. S., Read, R. J., Rice, L. M., Simonson, T. & Warren, G. L. (1998). *Acta Cryst.* **D54**, 905–921.
- Buth, G., Kölln, I. & Bartunik, H. D. (1996). *Rev. Sci. Instrum.* **67**, 3369.
- Cianci, M. *et al.* (2005). *J. Synchrotron Rad.* **12**, 455–466.
- Collaborative Computational Project, Number 4 (1994). *Acta Cryst.* **D50**, 760–763.
- Cowtan, K. (1994). *Jnt CCP4/ESF-EACBM Newsl. Protein Crystallogr.* **31**, 34–38.
- Dauter, Z., Dauter, M. & Rajashankar, K. R. (2000). *Acta Cryst.* **D56**, 232–237.
- DeLano, W. L. (2002). *The PyMOL Molecular Graphics System*. DeLano Scientific, San Carlos, CA, USA. (<http://www.pymol.org>.)
- Emsley, P. & Cowtan, K. (2004). *Acta Cryst.* **D60**, 2126–2132.
- Evans, G. & Pettifer, R. F. (2001). *J. Appl. Cryst.* **34**, 82–86.
- Girard, É., Stelter, M., Anelli, P. L., Vicat, J. & Kahn, R. (2003). *Acta Cryst.* **D59**, 118–126.
- Giuseppe, P. O., Neves, F. O., Nascimento, A. L. T. O. & Guimarães, B. G. (2008). *J. Struct. Biol.* **163**, 53–60.
- Golubev, A. M., Nagem, R. A. P., Brandão Neto, J. R., Neustroev, K. N., Eneyskaya, E. V., Kulminkaya, A. A., Shabalin, K. A., Savel'ev, A. N. & Polikarpov, I. (2004). *J. Mol. Biol.* **339**, 413–422.
- Grosse-Kunstleve, R. W. & Adams, P. D. (2003). *Acta Cryst.* **D59**, 1966–1973.
- Guzzo, C. & Farah, C. (2009). In preparation.
- Jiang, J. & Sweet, R. M. (2004). *J. Synchrotron Rad.* **11**, 319–327.
- Krauchenco, S., Nagem, R. A. P., da Silva, J. A., Marangoni, S. & Polikarpov, I. (2004). *Biochimie*, **86**, 167–172.
- La Fortelle, E. & Bricogne, G. (1997). *Methods Enzymol.* **276**, 472–493.
- Lamzin, V. S., Perrakis, A. & Wilson, K. S. (2001). *International Tables for Crystallography*, Vol. F, pp. 720–722. Dordrecht: Kluwer.
- Leslie, A. G. W. (1992). *Jnt CCP4/ESF-EAMCB Newsl. Protein Crystallogr.* **26**.
- McCoy, A. J., Grosse-Kunstleve, R. W., Adams, P. D., Winn, M. D., Storoni, L. C. & Read, R. J. (2007). *J. Appl. Cryst.* **40**, 658–674.
- McPhillips, T. M., McPhillips, S. E., Chiu, H.-J., Cohen, A. E., Deacon, A. M., Ellis, P. J., Garman, E., Gonzalez, A., Sauter, N. K., Phizackerley, R. P., Soltis, S. M. & Kuhn, P. (2002). *J. Synchrotron Rad.* **9**, 401–406.
- Miller, M. D., Phillips, G. N., White, M. A., Fox, R. O. & Craft, B. C. (2001). *AIP Conf. Proc.* **576**, 734–740.
- Murshudov, G. N., Vagin, A. A. & Dodson, E. J. (1997). *Acta Cryst.* **D53**, 240–255.
- Nagem, R. A. P., Ambrosio, A. L. B., Rojas, A. L., Navarro, M. V. A. S., Golubev, A. M., Garratt, R. C. & Polikarpov, I. (2005). *Acta Cryst.* **D61**, 1022–1030.
- Nagem, R. A. P., Colau, D., Dumoutier, L., Renault, J.-C., Ogata, C. & Polikarpov, I. (2002). *Structure*, **10**, 1051–1062.
- Nagem, R. A. P., Dauter, Z. & Polikarpov, I. (2001). *Acta Cryst.* **D57**, 996–1002.
- Nagem, R. A. P., Polikarpov, I. & Dauter, Z. (2003). *Methods Enzymol.* **374**, 120–137.
- Nagem, R. A. P., Rojas, A. L., Golubev, A. M., Korneeva, O. S., Eneyskaya, E. V., Kulminkaya, A. A., Neustroev, K. N. & Polikarpov, I. (2004). *J. Mol. Biol.* **344**, 471–480.
- Pal, A., Debreczeni, J. É., Sevana, M., Gruene, T., Kahle, B., Zeeck, A. & Sheldrick, G. M. (2008). *Acta Cryst.* **D64**, 985–992.
- Polikarpov, I., Perles, L. A., de Oliveira, R. T., Oliva, G., Castellano, E. E., Garratt, R. C. & Craievich, A. (1998). *J. Synchrotron Rad.* **5**, 72–76.
- Rodrigues, A. R. D., Craievich, A. F. & Gonçalves da Silva, C. E. T. (1998). *J. Synchrotron Rad.* **5**, 1157–1161.
- Rojas, A. L., Nagem, R. A. P., Neustroev, K. N., Arand, M., Adamska, M., Eneyskaya, E. V., Kulminkaya, A. A., Garratt, R. C., Golubev, A. M. & Polikarpov, I. (2004). *J. Mol. Biol.* **343**, 1281–1292.
- Schneider, T. R. & Sheldrick, G. M. (2002). *Acta Cryst.* **D58**, 1772–1779.
- Shi, W. *et al.* (2006). *J. Synchrotron Rad.* **13**, 365–372.
- Terwilliger, T. C. (2003). *Acta Cryst.* **D59**, 38–44.
- Wang, J., Dauter, M. & Dauter, Z. (2006). *Acta Cryst.* **D62**, 1475–1483.
- Welnak, C., Anderson, P., Khan, M., Singh, S. & Cerrina, F. (1992). *Rev. Sci. Instrum.* **63**, 865–868.
- Xie, J., Wang, L., Wu, N., Brock, A., Spraggon, G. & Schultz, P. G. (2004). *Nat. Biotechnol.* **22**, 1297–1301.